Letter

Anomalous noise spectra in a spin-exchange-relaxation-free alkali-metal vapor

K. Mouloudakis,[1,*] J. Kong,[2,*] A. Sierant,[1] E. Arkin,[2] M. Hernández Ruiz,[1]
R. Jiménez-Martínez,[3] and M. W. Mitchell[1,4]

[1]*ICFO - Institut de Ciències Fotòniques, The Barcelona Institute of Science and Technology, 08860 Castelldefels (Barcelona), Spain*
[2]*Department of Physics, Hangzhou Dianzi University, Hangzhou 310018, China*
[3]*FieldLine Industries, Boulder, Colorado 80303, USA*
[4]*ICREA - Institució Catalana de Recerca i Estudis Avançats, 08010 Barcelona, Spain*

(Received 31 July 2023; revised 6 December 2023; accepted 28 March 2024; published 30 April 2024)

We perform spin-noise spectroscopy on an unpolarized ^{87}Rb vapor in the spin-exchange-relaxation-free (SERF) regime. We observe noise spectral distributions that deviate strongly from Lorentzian models that accurately describe lower-density regimes. For example, at magnetic fields of $\sim$1 μT and ^{87}Rb densities of $\gtrsim 1 \times 10^{14}$ atoms/cm^3 we observe an asymmetric spin-noise distribution in which the resonance line is depleted by about half its power, with the diverted power becoming a broad spectral component that could be mistaken for optical shot noise. The results are in good agreement with recent models accounting for correlations between the ground hyperfine states. We discuss implications for quantum sensing and absolute noise calibration in spin squeezing and entanglement detection. The results suggest similarly anomalous spectra for other noise spectroscopies, when noise mechanisms are not aligned with system dynamics.

DOI: 10.1103/PhysRevA.109.L040802

Noise spectra, obtained by continuous observation of a system of interest without active excitation, provide information about the dynamics of nearly undisturbed systems close to natural thermal equilibrium [1,2]. In recent years, noise spectroscopies have been developed for electronic [3], optomechanical [4], biological [5], and especially spin systems [6,7], where the technique is known as spin-noise spectroscopy [2,8–19]. The interpretation of noise spectra benefits from weak thermal excitation, which ensures a linear response regime and allows calculation of equilibrium variances from thermodynamic principles. Under ideal detection, noise spectra obey an "area conservation rule" (shape-independent net noise power) and a "no-go theorem" (vanishing cross-correlations) [9]. These allow absolute calibration of the participating spin number [20] and the identification of Lorentzian spectral features with collective or single-particle modes, and other feature shapes with inhomogeneous broadening or more complex dynamics [9,21]. Optically detected noise spectra also provide absolute calibration of the photon shot noise (PSN) [22,23].

Here we report anomalous spin-noise spectra that do not fit the above description. Our spin system is a high-density alkali-metal vapor that can be tuned from the spin-exchange (SE)-relaxation regime into the spin-exchange-relaxation-free (SERF) regime [24]. In the SERF regime, SE collisions and hyperfine interactions dominate the spin dynamics, leading to line narrowing of the magnetic resonances and a corresponding boost to the sensitivity [25–28]. The SERF effect is employed in biomagnetism detection [29], inertial sensors [30], and tests of fundamental physics [31]. Experiments show that SERF media support and preserve nonclassical spin correlations, i.e., entanglement and spin squeezing [32]. Theory suggests that SE collisions can preserve other nonclassical states over long timescales [33].

Using the quantum structure of alkali-metal spin states, spin dynamics [34–36], and the regression theorem [37], recent theory predicts spin-noise spectra in the SERF regime [38]. In agreement with this theory, we observe the following anomalous behaviors: non-Lorentzian noise spectral features in a linear homogeneous system, flat noise backgrounds not due to PSN, and an apparent (but not real) violation of the area conservation law. We identify the underlying cause of these line-reshaping phenomena in a misalignment of the dynamical modes and the SE noise modes that drive them.

The experimental setup is shown in Fig. 1(a). Isotopically enriched ^{87}Rb and 0.12 amagat of N_2 buffer gas are held in a cylindrical cell of 12.7-mm diameter and 30-mm internal length, with antireflection-coated windows of 5-mm thickness. The cell is placed at the center of a cylindrical, four-layer, mu-metal magnetic shield. Solenoid and shim coils are used to produce a homogeneous dc magnetic field $\mathbf{B} = (B, 0, 0)$ along the $\hat{\mathbf{x}}$ direction. A ceramic oven, intermittent Joule heating, and a thermocouple are used to control the cell temperature. An external cavity diode laser produces a linearly polarized 795-nm beam detuned 46 GHz to the blue of the D_1 line of ^{87}Rb, monitored with a wavelength meter. The laser output, propagating along $\hat{\mathbf{z}}$, is spatially filtered with a single-mode fiber to produce a Gaussian beam with the effective area $A_{\text{eff}} \equiv L[\int I(x,y,z)\,dx\,dy]^2 / \int I^2(x,y,z)\,dx\,dy\,dz \approx 1.5$ mm^2, where $I(x,y,z)$ is the intensity of the Gaussian beam, measured with a beam profiler, and L is the length of the cell [40]. The effective number of atoms probed by the laser beam is $N_{\text{at}} = nA_{\text{eff}}L$, where n is the alkali-metal number density.

*These authors contributed equally to this work.

 ©2024 American Physical Society

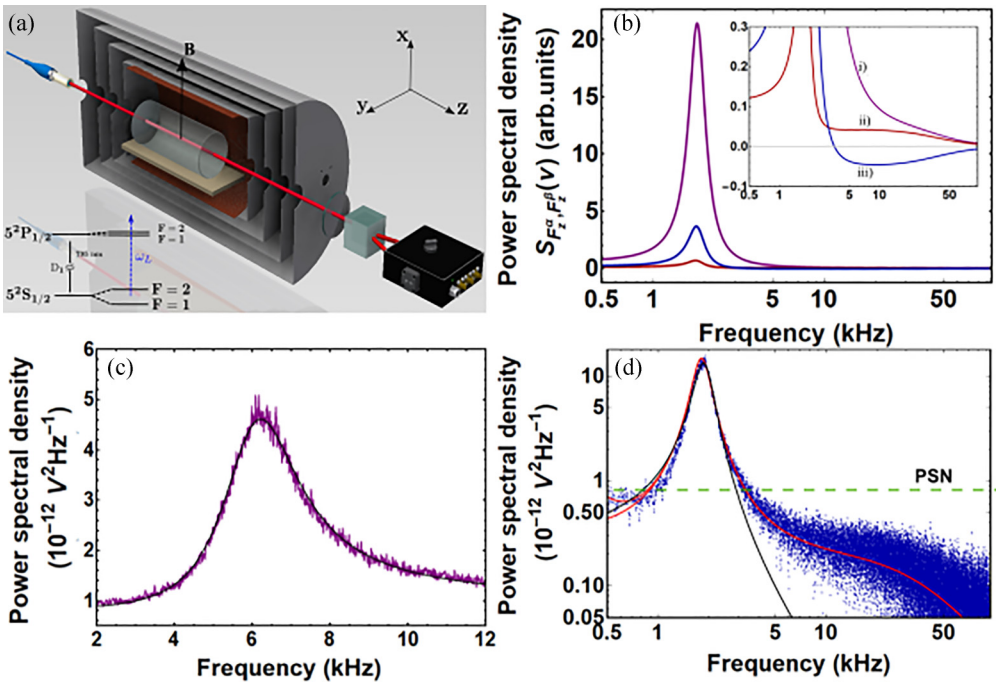

FIG. 1. Experimental setup and representative spectra. (a) Schematic representation of the experimental setup (see text). (b) Predicted non-Lorentzian spin-noise contributions (i) $S_{\hat{F}_z^a,\hat{F}_z^a}(\nu)$, (ii) $S_{\hat{F}_z^b,\hat{F}_z^b}(\nu)$, (iii) $S_{\hat{F}_z^a,\hat{F}_z^b}(\nu)$, and $S_{\hat{F}_z^b,\hat{F}_z^a}(\nu)$, computed using Eq. (6) and experimentally relevant parameters: $R_{se} \approx 3.02 \times 10^5\ s^{-1}$ and $R_{sd} \approx 0.03 \times 10^5\ s^{-1}$, corresponding to 3.4×10^{14} atoms/cm^3 and temperature $T = 169\,^\circ$C. The magnetic field is $B = 385$ nT along the $\hat{\mathbf{x}}$ direction. (c) Example of a non-Lorentzian spectrum at a magnetic field of $B \approx 1292$ nT fitted to a Lorentzian plus dispersive curve (see Ref. [39] for details). (d) Spin-noise spectra acquired at a magnetic field of $B = 385$ nT and a number density of $n \approx 3.4 \times 10^{14}$ atoms/cm^3. The mean PSN level is depicted by the green dashed line and has been subtracted from the spectrum. Data are fitted by a Lorentzian model (black solid line) and Eq. (1) (red solid lines) with and without "1/f-noise". The departure from the Lorentzian spectrum is demonstrated.

Both the detuning of the light and the atomic 2.4-GHz full width at half maximum (FWHM) pressure-broadened optical linewidth are larger than the 0.8-GHz hyperfine splitting of the excited state, so tensor polarizability effects are expected to be negligible [41]. The transmitted light is detected by a balanced polarimeter comprised of a half-waveplate, a Wollaston prism, and an amplified differential photodetector (PD). The PD signal is recorded by a 24-bit digitizer for later processing.

The experimentally obtained noise spectra are of the form

$$S_{\rm opt}(\nu) = S_{\rm psn} + S_{1/f}(\nu) + S_{\rm el}(\nu) + S_{\rm at}(\nu), \tag{1}$$

where the contribution from the photon shot noise (PSN) is $S_{\rm psn} = 2G^2 q_e r P \approx 0.91 \times 10^{-12}\ {\rm V^2\,Hz^{-1}}$, with $q_e \approx 1.6 \times 10^{-19}$ C being the electron charge, $r \approx 0.52\ {\rm AW^{-1}}$ at 795 nm the PD responsivity, $G = 1 \times 10^5\ {\rm VA^{-1}}$ the transimpendance gain of the PD, and $P \approx 550$ μW the laser power reaching the polarimeter. $S_{1/f} = \zeta^2 \nu^{-\beta}$, $\beta > 0$, is the "1/f noise" with strength ζ^2, and $S_{\rm el}(\nu)$ is the electronic noise of the PD and the acquisition system, which in practice is about 20 dB below the PSN background. The last term in Eq. (1) is the atomic spin-noise spectrum, presenting a resonance feature at the spin-precession frequency. The spin-noise power of the thermal state is a readily available noise reference and has been used in noise calibration for spin squeezing [42] and entanglement detection [32] experiments. We note that for frequencies above 0.5 kHz, $S_{1/f}(\nu)$ is negligible; thus, in the analysis that follows $S_{\rm opt}(\nu)$ is approximated as $S_{\rm opt}(\nu) \approx S_{\rm at}(\nu) + S_{\rm psn}$.

To model the atomic spectra we employ the Ornstein-Uhlenbeck approach as derived in Ref. [38] and further discussed in Ref. [39]. In this model, the spectra result from the stochastic dynamics of the hyperfine collective spin vectors $\hat{\mathbf{F}}^\alpha(t)$, $\alpha \in \{a = I + 1/2, b = I - 1/2\}$, governed by

$$d\hat{\mathbf{X}}(t) = A\hat{\mathbf{X}}(t)dt + Qd\hat{\mathbf{W}}(t), \tag{2}$$

where $\hat{\mathbf{X}} \equiv [\hat{F}_x^a, \hat{F}_y^a, \hat{F}_z^a, \hat{F}_x^b, \hat{F}_y^b, \hat{F}_z^b]^T$, A is the drift matrix, Q is the noise strength matrix, and $d\hat{\mathbf{W}}$ is a length-six vector of independent Wiener increments [39]. For such processes, with real A and Q, the power spectral density matrix is [37]

$$S_{\hat{\mathbf{X}},\hat{\mathbf{X}}}(\omega) = -\frac{1}{2\pi}(A + i\omega\mathbb{1})^{-1} QQ^T (A^T - i\omega\mathbb{1})^{-1}, \tag{3}$$

where $\mathbb{1}$ is the 6×6 identity matrix. In equilibrium, QQ^T is directly related to A and to the steady-state, equal-time covariance matrix $\mathcal{R}_{\hat{\mathbf{X}},\hat{\mathbf{X}}}(0)$ by

$$QQ^T = A\mathcal{R}_{\hat{\mathbf{X}},\hat{\mathbf{X}}}(0) + \mathcal{R}_{\hat{\mathbf{X}},\hat{\mathbf{X}}}(0)A^T, \tag{4}$$

where

$$\mathcal{R}_{\hat{F}_i^\alpha,\hat{F}_j^\beta}(0) = \delta_{ij}\delta_{\alpha\beta}\frac{f^\alpha(f^\alpha+1)(2f^\alpha+1)}{6(2I+1)}N_{\rm at}. \tag{5}$$

Here $N_{\rm at}$ is the number of atoms contributing to the spectrum and f^α is the single-atom hyperfine spin value [38]. In this way, it is possible to compute fluctuation spectra for the distinct hyperfine (α) components. As evident from Eqs. (2), (4), and (5), the fluctuating drive term $Qd\hat{\mathbf{W}}(t)$ originates in the discreteness of the atomic spin. The equal-time covariance,

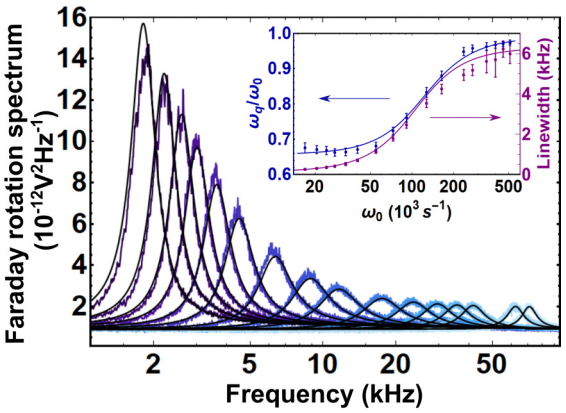

FIG. 2. Single-sided power spectral density (PSD) of the polarimeter signal (in volts, conversion to rotation angle 35 mrad/V) for transverse magnetic fields ranging from 280 nT to 12 μT while the vapor cell is maintained at approximately 169 °C. Each spectrum shows the linear average [39] of 150 spectra, each computed on a 0.5-s acquisition with a sampling rate of 200 kSa s^{-1}. A 20-Hz (ten-bin) boxcar smoothing has also been applied [8]. Black solid lines: Fit of Eq. (1) (excluding 1/f and electronic noise) to the observed spectra (see text). Inset: The left axis shows spin-noise precession frequency ω_q normalized to $\omega_0 = g_s\mu_B B/[\hbar(2I+1)]$ versus ω_0 known by calibration of the coils at low density [39]. The right axis shows the spin-noise linewidth (half width at half maximum) versus ω_0. Data are obtained by fitting the spectra with a distorted Lorentzian (see text). Error bars show ±1 standard deviation in the fit estimation parameters over 150 acquisitions. The blue (purple) solid line shows Im[λ] (Re[λ]) of the eigenvalues of the drift matrix A, as given by Eq. (7) of Ref. [39]. The parameters are discussed in the main text.

Eq. (5), describes a separable state, as befits the mean-field description [38].

A Faraday rotation signal from such a medium has the power spectral density [39]

$$S_{\rm at}(\nu) = \mathcal{A}\, r^2 G^2 P^2 \big[g_a^2 S_{\hat{F}_z^a,\hat{F}_z^a}(\nu) + g_b^2 S_{\hat{F}_z^b,\hat{F}_z^b}(\nu) - g_a g_b \big(S_{\hat{F}_z^a,\hat{F}_z^b}(\nu) + S_{\hat{F}_z^b,\hat{F}_z^a}(\nu)\big)\big], \quad (6)$$

where $\mathcal{A}$ is a unitless scale factor and g_α is a detuning-dependent coupling proportional to the vector polarizability for the hyperfine state α.

Cross-correlations between the two ground-state hyperfine levels allow for the $g_a g_b$ term in Eq. (6) to partially cancel the g_a^2 and g_b^2 terms, thereby distorting the spectra and affecting the distribution of spin-noise power. The non-Lorentzian character of these spectra is illustrated in Figs. 1(b) and 1(c). Representative spin-noise spectra, acquired as a function of transverse bias field, are shown in Fig. 2.

We fit the observed spectra with $S_{\rm opt}(\nu) = S_{\rm at}(\nu) + S_{\rm psn}$, with $S_{\rm at}(\nu)$ from Eq. (6) and photon shot noise $S_{\rm psn} = 0.91 \times 10^{-12}$ V^2 Hz^{-1} from an independent measurement. The magnetic field is inferred from the current in the B_x coil, previously calibrated by spin-noise spectroscopy at low density [39]. A simultaneous fit to all spectra finds best-fit parameters $R_{\rm se} = 3.02 \times 10^5$ s^{-1}, $R_{\rm sd} = 0.03 \times 10^5$ s^{-1}, $R = 400$ s^{-1}, and $\mathcal{A} = 2.3$. These are respectively the rates of spin-exchange, spin-destruction, and spin-depolarizing processes as defined in Refs. [39,43]. The fitted spectra are shown as black lines in Fig. 2 and agree well except at the lowest field strengths. Deviations from Eq. (6) at low field are expected due to imperfect compensation of remanent fields, the $S_{1/f}(\nu)$ contribution, and diffusion. A complete model accounting for both spin-exchange and atomic diffusion effects is still missing from the literature; however, diffusion alone has been studied in Refs. [15,19]. From the fitted value of the spin-exchange rate, the 169 °C temperature of the vapor, and the 1.9×10^{-14} cm^2 SE cross section [44], we infer an alkali-metal number density of 3.4×10^{14} atoms/cm^3.

To visualize the "slowing-down" of the spin precession and the linewidth reduction, in Fig. 2 (inset) we compare the observed resonance frequency and linewidth from distorted-Lorentzian fits to individual spectra [39] against the predictions of Eq. (6) with the above fit parameters. As described in Ref. [39], the predicted values can be computed from the real and imaginary parts of the eigenvalues of the drift matrix A. This extends the results of Ref. [26] to account for spin-destruction and spin-depolarizing processes, for any alkali-metal species. We now study the spectral redistribution of spin-noise power across the transition from the SE-dominated to the SERF regime. The total atomic noise power in this state is given by

$$\int_0^\infty S_{\rm at}(\nu)d\nu = \frac{1}{2}\mathcal{A} r^2 G^2 P^2 \big[g_a^2 {\rm var}(F^a) + g_b^2 {\rm var}(F^b)\big], \quad (7)$$

where ${\rm var}(F^\alpha)$, $\alpha \in [a,b]$, are given by Eq. (5). Since our acquisition is limited by a 100-kHz Nyquist frequency, the experimentally obtained noise is only a portion of Eq. (7), as discussed in Ref. [39]. We stress that the noise in Eq. (7) is independent of the magnetic-resonance parameters and depends only on the number of probed atoms, the probe intensity and detuning, and the optical linewidth.

In the SERF regime, the predicted spectra are non-Lorentzian, with a significant portion of spin noise spread over the high-frequency part of the spectrum. To demonstrate this, we acquire spectra under a fixed transverse field of $B = 918$ nT, while the alkali-metal number density is varied across the transition from slow SE ($R_{\rm se} \ll \omega_0$) to rapid SE ($R_{\rm se} \gg \omega_0$) (see Fig. 3, inset). We numerically integrate the observed spectra to compute

$$\int_{\nu_{\rm low}}^{\nu_{\rm br}} S_{\rm at}(\nu)d\nu \Big/ \int_{\nu_{\rm low}}^{\nu_{\rm bw}} S_{\rm at}(\nu)d\nu, \quad (8)$$

which describes the fraction of the observed power below the cutoff frequency $\nu_{\rm br}$. We choose $\nu_{\rm bw} = 95$ kHz as the upper limit and $\nu_{\rm low} = 0.5$ kHz as the lower limit of integration in order to avoid distortions in the noise power due to the digitizer's antialiasing filter and the 1/f noise, respectively. The cutoff frequency $\nu_{\rm br} = 20$ kHz is chosen to be a few FWHM above resonance, so that, were the line Lorentzian, nearly all the spin noise would be below the cutoff frequency. It is seen in Fig. 3 that at low densities nearly all of the atomic noise is below $\nu_{\rm br}$, whereas at higher densities, in the SERF regime, nearly 50% of the noise shifts above $\nu_{\rm br}$ [45]. The choice of $\nu_{\rm br}$ and the contributions of different hyperfine levels are discussed in Ref. [39].

This line reshaping, if not accounted for, can produce systematic errors in calibration, in estimation of both the atom

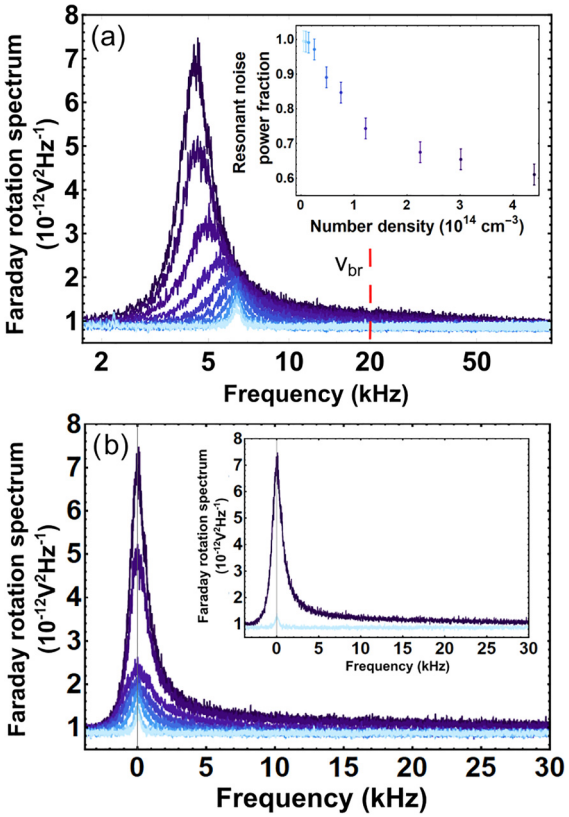

FIG. 3. Non-Lorentzian spectra and apparent (but not real) violation of the area conservation law. (a) Spin-noise spectra (single-sided PSD) as a function of the ^{87}Rb number density for a fixed magnetic field of $B = 918$ nT. Each spectrum shows the linear average of 100 spectra. Long high-frequency tails are apparent. Inset: Resonant noise power fraction as a function of number density as calculated using Eq. (8). The cutoff frequency $\nu_{\rm br}$ at 20 kHz is indicated by the red dashed line. Error bars show ± 1 standard deviation in the numerical integration over 100 acquisitions. (b) For visualizing the power redistribution, the spin-noise resonances of Fig. 3(a) are plotted with the frequency axis shifted so that each is centered at 0. Curves are plotted for a constant field $B = 918$ nT and varying number density. The values for the number densities are reported in Ref. [39]. The inset shows spin-noise resonances for the lower (5.1×10^{12} / cm^3) and higher (4.4×10^{14} / cm^3) atomic densities acquired.

number from the integrated spin noise and the photon shot noise based on the flat, high-frequency tail of $S_{\rm at}(\nu)$. Although we study the spin-unpolarized regime, similar effects can be expected for weakly polarized ensembles [16]. Several magnetometry strategies obtain signals from spin precession at ω_q and would thus benefit from the noise reduction identified here. This noise advantage exists in addition to the well-known coherence-time advantage in the SERF regime [24,27,28].

The observed line reshaping is not specific to the SERF regime or even to spin systems. Equation (2), an inhomogeneous linear equation, describes many physical systems. The eigenvectors $\mathbf{v}_i$ and eigenvalues $\lambda_i = i\omega_i - \Gamma_i$ of A describe modes, necessarily Lorentzian, of response to the drive $Qd\hat{\mathbf{W}}$. If the noise is aligned to these modes, i.e., if $Qd\hat{\mathbf{W}}(t) = \sum_i q_i \mathbf{v}_i dW_i(t)$, where $dW_i(t)$ are independent Wiener increments and q_i are scalar weights, then each mode fluctuates independently and the spectrum will be a sum of Lorentzian features. If $Qd\hat{\mathbf{W}}$ is not so aligned, it produces intramode correlations, as in Eq. (6), and consequent spectral line distortion [39]. In this way, noise spectroscopy probes both the medium's dynamical structure and its noise sources.

In conclusion, we have measured and characterized the spin noise of a thermal ^{87}Rb in the transition from the SE-dominated to the SERF regimes. We observe anomalous noise line shapes arising from strong coupling of the ground hyperfine spins in the SERF regime. The line reshaping notably reduces the power in the resonant peak and produces a broadband component that imitates photon shot noise. The results validate recent theoretical models, improve the accuracy of thermal-state-based noise calibration for spin squeezing and entanglement generation, and suggest a hyperfine-correlation-induced reduction in fundamental quantum noise for optically pumped magnetometers operating in the SERF regime.

We thank G. Vasilakis, J. Kołodyński, and V. G. Lucivero for useful discussions. J.K. and E.A. acknowledge support from the National Natural Science Foundation of China (NSFC) (Grants No. 12374463 and No. 11935012). K.M. acknowledges support from Grant No. FJC2021-047840-I funded by MCIN/AEI/10.13039/501100011033 and by the European Union "NextGenerationEU/PRTR." M.H.R. acknowledges support from Ayuda PRE2021-098880 financiada por MCIN/AEI/10.13039/501100011033 y por el FSE+. M.H.R., A.S., K.M., and M.W.M. acknowledge the Spanish Ministry of Science MCIN with funding from NextGenerationEU (PRTR-C17.I1) and Generalitat de Catalunya, "Severo Ochoa" Center of Excellence CEX2019-000910-S; projects SAPONARIA (PID2021-123813NB-I00) and MARICHAS (PID2021-126059OA-I00) funded by MCIN/AEI/10.13039/501100011033/FEDER, EU; Generalitat de Catalunya through the CERCA program; Agència de Gestió d'Ajuts Universitaris i de Recerca Grant No. 2017-SGR-1354; Fundació Privada Cellex; Fundació Mir-Puig; and The European Commission Project OPMMEG (Grant No. 101099379).

[1] A. Einstein, Ann. Phys. **322**, 549 (1905).
[2] E. B. Alexandrov and V. S. Zapasskii, Sov. Phys. JETP **54**, 64 (1981).
[3] W.-K. Tse, A. Saxena, D. L. Smith, and N. A. Sinitsyn, Phys. Rev. Lett. **113**, 046602 (2014).
[4] D. Yu and F. Vollmer, Commun. Phys. **5**, 61 (2022).
[5] G. Zheng, X. P. A. Gao, and C. M. Lieber, Nano Lett. **10**, 3179 (2010).
[6] G. M. Müller, M. Oestreich, M. Römer, and J. Hübner, Physica E **43**, 569 (2010).
[7] S. A. Crooker, D. G. Rickel, A. V. Balatsky, and D. L. Smith, Nature (London) **431**, 49 (2004).

[8] V. G. Lucivero, A. Dimic, J. Kong, R. Jiménez-Martínez, and M. W. Mitchell, Phys. Rev. A **95**, 041803(R) (2017).

[9] N. A. Sinitsyn and Y. V. Pershin, Rep. Prog. Phys. **79**, 106501 (2016).

[10] G. E. Katsoprinakis, A. T. Dellis, and I. K. Kominis, Phys. Rev. A **75**, 042502 (2007).

[11] Y. Wen, X. Li, G. Zhang, and K. Zhao, Phys. Rev. A **104**, 063708 (2021).

[12] V. G. Lucivero, R. Jiménez-Martínez, J. Kong, and M. W. Mitchell, Phys. Rev. A **93**, 053802 (2016).

[13] S. Song, M. Jiang, Y. Qin, Y. Tong, W. Zhang, X. Qin, R.-B. Liu, and X. Peng, Phys. Rev. Appl. **17**, L011001 (2022).

[14] M. Oestreich, M. Römer, R. J. Haug, and D. Hägele, Phys. Rev. Lett. **95**, 216603 (2005).

[15] V. G. Lucivero, N. D. McDonough, N. Dural, and M. V. Romalis, Phys. Rev. A **96**, 062702 (2017).

[16] V. Shah, G. Vasilakis, and M. V. Romalis, Phys. Rev. Lett. **104**, 013601 (2010).

[17] G. Vasilakis, H. Shen, K. Jensen, M. Balabas, D. Salart, B. Chen, and E. S. Polzik, Nat. Phys. **11**, 389 (2015).

[18] R. Jiménez-Martínez, J. Kołodyński, C. Troullinou, V. G. Lucivero, J. Kong, and M. W. Mitchell, Phys. Rev. Lett. **120**, 040503 (2018).

[19] R. Shaham, O. Katz, and O. Firstenberg, Phys. Rev. A **102**, 012822 (2020).

[20] M. Koschorreck, M. Napolitano, B. Dubost, and M. W. Mitchell, Phys. Rev. Lett. **104**, 093602 (2010).

[21] J. Meinel, V. Vorobyov, P. Wang, B. Yavkin, M. Pfender, H. Sumiya, S. Onoda, J. Isoya, R.-B. Liu, and J. Wrachtrup, Nat. Commun. **13**, 5318 (2022).

[22] F. Wolfgramm, A. Cerè, F. A. Beduini, A. Predojević, M. Koschorreck, and M. W. Mitchell, Phys. Rev. Lett. **105**, 053601 (2010).

[23] C. Troullinou, R. Jiménez-Martínez, J. Kong, V. G. Lucivero, and M. W. Mitchell, Phys. Rev. Lett. **127**, 193601 (2021).

[24] I. M. Savukov and M. V. Romalis, Phys. Rev. A **71**, 023405 (2005).

[25] W. Happer and H. Tang, Phys. Rev. Lett. **31**, 273 (1973).

[26] W. Happer and A. C. Tam, Phys. Rev. A **16**, 1877 (1977).

[27] J. C. Allred, R. N. Lyman, T. W. Kornack, and M. V. Romalis, Phys. Rev. Lett. **89**, 130801 (2002).

[28] I. K. Kominis, T. W. Kornack, J. C. Allred, and M. V. Romalis, Nature (London) **422**, 596 (2003).

[29] E. Boto, S. S. Meyer, V. Shah, O. Alem, S. Knappe, P. Kruger, T. M. Fromhold, M. Lim, P. M. Glover, P. G. Morris, R. Bowtell, G. R. Barnes, and M. J. Brookes, NeuroImage **149**, 404 (2017).

[30] T. W. Kornack, R. K. Ghosh, and M. V. Romalis, Phys. Rev. Lett. **95**, 230801 (2005).

[31] J. Lee, A. Almasi, and M. Romalis, Phys. Rev. Lett. **120**, 161801 (2018).

[32] J. Kong, R. Jiménez-Martínez, C. Troullinou, V. G. Lucivero, G. Tóth, and M. W. Mitchell, Nat. Commun. **11**, 2415 (2020).

[33] K. Mouloudakis and I. K. Kominis, Phys. Rev. A **103**, L010401 (2021).

[34] S. Appelt, A. B.-A. Baranga, C. J. Erickson, M. V. Romalis, A. R. Young, and W. Happer, Phys. Rev. A **58**, 1412 (1998).

[35] O. Katz, R. Shaham, and O. Firstenberg, PRX Quantum **3**, 010305 (2022).

[36] J. L. Sørensen, J. Hald, and E. S. Polzik, Phys. Rev. Lett. **80**, 3487 (1998).

[37] C. Gardiner, *Stochastic Methods*, 4th ed. (Springer, Berlin, 2009).

[38] K. Mouloudakis, G. Vasilakis, V. G. Lucivero, J. Kong, I. K. Kominis, and M. W. Mitchell, Phys. Rev. A **106**, 023112 (2022).

[39] See Supplemental Material at http://link.aps.org/supplemental/10.1103/PhysRevA.109.L040802 for more details.

[40] M. H. Schleier-Smith, I. D. Leroux, and V. Vuletic, Phys. Rev. Lett. **104**, 073604 (2010).

[41] W. Happer and B. S. Mathur, Phys. Rev. **163**, 12 (1967).

[42] T. Fernholz, H. Krauter, K. Jensen, J. F. Sherson, A. S. Sørensen, and E. S. Polzik, Phys. Rev. Lett. **101**, 073601 (2008).

[43] We distinguish between relaxation processes that depolarize only the electron spin and leave the nuclear spin state intact ("spin destruction") and processes that thermalize both the nuclear and the electron spins ("spin depolarization") [39].

[44] S. J. Seltzer, *Developments in Alkali-Metal Atomic Magnetometry* (Princeton University, Princeton, NJ, 2008).

[45] In the SE regime, the transverse projections of $\mathbf{F}_a$ and $\mathbf{F}_b$ each precess at the Larmor frequency, whereas in SERF, only the transverse projection of the net spin $\mathbf{F}_a + \mathbf{F}_b$ precesses in this way. This suggests that the *number* of Larmor-precessing degrees of freedom is important in determining the spin-noise power distribution.